ACS OMEGA

Article

Cite This: ACS Omega 2019, 4, 10293−10301

http://pubs.acs.org/journal/acsodf

Tuning the Electronic and Magnetic Properties of Graphene Flake Embedded in Boron Nitride Nanoribbons with Transverse Electric Fields: First-Principles Calculations

Zhaoyong Guan,*[,†,‡] Shuang Ni,[§] and Shuanglin Hu[∥]

[†]School of Chemistry and Chemical Engineering, Shandong University, Jinan 250100, P. R. China

[‡]Department of Physics, Tsinghua University, Beijing 100084, P. R. China

[§]Research Center of Laser Fusion and [∥]Institute of Nuclear Physics and Chemistry, China Academy of Engineering Physics, Mianyang, Sichuan 621900, P. R. China

Supporting Information

ABSTRACT: The electronic and magnetic properties of h-BN nanoribbions embedded with graphene nanoflakes (CBNNRs) are systematically studied by ab initio calculations. The CBNNRs with zigzag or armchair edges are all bipolar magnetic semiconductors (BMSs). The band gaps of zigzag CBNNRs (zCBNNRs) change linearly with the transverse electric field (*E*-field) for the first-order Stark effect, whereas for the armchair CBNNRs (aCBNNRs), the band gaps vary quadratically with the *E*-field for the second-order Stark effect. For zCBNNRs and aCBNNRs, they could transform from BMS to spin gapless semiconductor (SGS), metal, and half-metal (HM) under different transverse *E*-fields. The CBNNRs may transform into a semiconductor or HM, under the same *E*-fields, depending on the position of graphene flakes. The CBNNRs introduce local magnetic moment at carbon atoms, and the magnetic moment is determined by the size of the graphene flakes. These observations open the door to applications of CBNNRs in spintronic devices.

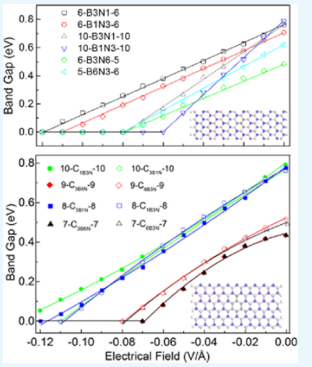

1. INTRODUCTION

In 2004, Geim et al. successfully isolated graphene by using the micromechanical exfoliation method[1] and graphene has worked as an attractive candidate material for electro-mechanical resonators, flexible electronic circuitry, ultra-capacitors, stable field emitters, and as fillers for electrically conducting flexible nanocomposites.[2−4] Researchers started to explore hexagonal boron nitride (h-BN),[5] since two-dimensional (2D) h-BN nanosheets have distinct advantages compared with graphene;[6,7] for example, they are electrically insulating (a band gap of 5 eV), have profound chemical and thermal stabilities,[5] but at the same time are thermally conductive and mechanically robust as their C counterparts.[6] So the 2D h-BN nanosheet is also named "white" graphene.[8] Combining carbon with its neighboring atoms in the periodic table (boron and nitrogen) offers a host of different hybrid hexagonal CBN nanosystems.[9,10] As discussed above, graphene is a semimetal[1] whereas h-BN is an insulator with a wide band gap.[5,7] The h-CBN structures may have energy band gaps smaller than that of h-BN and can be continuously tuned by changing the concentration and arrangement of the C and BN.[9,10] These attractive physical properties as well as chemical inertness motivated the attempt to produce h-CBN. Various approaches, including ion beam-assisted deposition,[11] magnetron sputtering,[12] radio frequency plasma enhanced pulsed-laser deposition,[13] excimer laser annealing,[14] and chemical vapor deposition (CVD),[12,15−22] were used to grow the h-CBN thin films. In fact, the phase separation is the most challenging obstacle for producing crystalline bulks and films.[23−32] Mixtures of pure BN and graphene domains coexist in these compounds.[28,29,33,34]

A breakthrough on the controlled CVD preparation and characterization of epitaxial CBN nanosheets has recently been reported by Ci et al., who developed a systematic route to synthesize 2D CBN hybrid structures consisting of a patchwork of BN and C nanodomains. He also has synthesized the graphene flakes with a triangular shape doped into the h-BN monolayer and confirmed in the scanning tunneling microscopy.[35] The doped electron or hole could effectively tune the formation energy of complex CBN structures.[36] The triangular graphene flakes are synthesized highly crystalline hybrid BNC sheets by Han et al., and the results reveal that embedded C2 or C6 units in BN-dominated regions energetically are the most favorable.[37] In 2013, Lu et al. demonstrated that metal substrate-catalyzed substitutional exchange of h-BN by carbon atoms presented a route for doping and alloying under nonequilibrium conditions.[38] In 2014, Liu et al. developed an ingenious method and he found an abrupt one-dimensional (1D) interface or a boundary with the atmospheric-pressure chemical vapor deposition.[39] Wei et al. have recently reported the C-doping of various BN nanostructures, including BN nanotubes, BN nanosheets, and

Received: March 18, 2019
Accepted: April 24, 2019
Published: June 13, 2019

DOI: 10.1021/acsomega.9b00752
ACS Omega 2019, 4, 10293−10301

BNNRs by electron beam irradiation in the presence of solid paraffin wax as the carbon source with an electron microscope.[40] Other researchers also synthesized all kinds of structures.[41−43]

There are is a lot of experimental progress, but there is no systematic work about one-dimensional (1D) CBNNRs (now only 2D triangular graphene flakes embedded in h-BN[37]). In this work, we discuss 1D superlattices where carbon atom-formed nanoflakes are embedded in the BNNRs. In this article, by using the first-principles method, we investigate the geometric, electronic, and magnetic properties of both armchair and zigzag CBNNRs under a transverse *E*-field. We study electronic and magnetic properties using the Perdew−Burke−Ernzerhof (PBE) functional,[44] then further using the transverse *E*-field to tune their electronic and magnetic properties. We find that both zigzag and armchair BNNRs doped with graphene flakes are typical BMS,[45] for the first time, and the states near the Fermi level are mainly contributed by the carbon atoms. The electronic properties of zigzag and armchair CBNNRs change from BMS to semiconductor, SGS,[46−48] to half-metal[49−52] with different transverse *E*-fields. The band gaps of zigzag CBNNRs follow a linear relationship with the *E*-field for the first-order Stark effect,[53−55] no matter what is the width of the CBNNRs, whereas band gap of armchair CBNNRs varies quadratically for the second-order Stark effect.[53−55] The total magnetic moment (MM) is determined by the size of the graphene flakes.

2. COMPUTATIONAL DETAILS

The calculations on the CBNNRs are performed by using a numerical radial function basis set DMol3 package[56,57] based on the density functional theory under the generalized gradient approximation with the Perdew−Burke−Ernzerhof (PBE) functional.[44] The basis set is adopted on the basis of the double numerical atomic orbitals augmented by polarization functions, which are comparable to Gaussian 6-31G** sets. The vacuum space in the *z* direction is set as large as 20 Å to avoid the interactions between the periodic images. The real-space global cutoff radius is set to 4.3 Å. For geometry optimization, total energy, and band structure calculations, 20, 60, and 100 Monkhost−Pack *k*-points[58] are adopted to sample the 1D Brillouin zones, respectively. The calculations used are all electron ones considering scalar relativistic corrections. As for the self-consistent electronic structure calculations, the convergence criterions on the energy and electron density are set to be 1×10^{-6} au (1 Hartree = 1 au = 27.21 eV). Geometry optimizations are performed with convergence criteria of 1×10^{-3} au/Å on the gradient, 5×10^{-3} Å on the displacement, and 1×10^{-5} au on the total energy. The h-BN and BNNRs are used as testing systems to check the accuracy of our procedure. The B−N bond length in h-BN is calculated to be 1.45 Å, which is consistent with the experimental measured value.[5,7] The calculated band gaps of 18-zBNNR and 18-aBNNR are 3.72 and 4.53 eV, respectively, which also agree well with the previous results.[59] The dipole correction is considered in the following calculation. The transverse electric field in a supercell is simulated with a periodic saw tooth-type potential, which is homogeneous along the ribbon edges, perpendicular to the ribbon edge. BNNR has two kinds of sublattice named α and β lattice, seen at the position of B and N atoms, respectively. In this research, some of the boron or nitrogen atoms are replaced by the carbon atoms with triangular geometry. Monolayer graphene could work as a candidate for doping h-BN, as h-BN and graphene have quite similar bond lengths and geometries (planar hexagonal geometry).[10]

3. RESULTS AND DISCUSSION

3.1. Geometry of the CBNNRs. We first optimize the geometry of CBNNRs, as shown in Figure 1a,b, respectively.

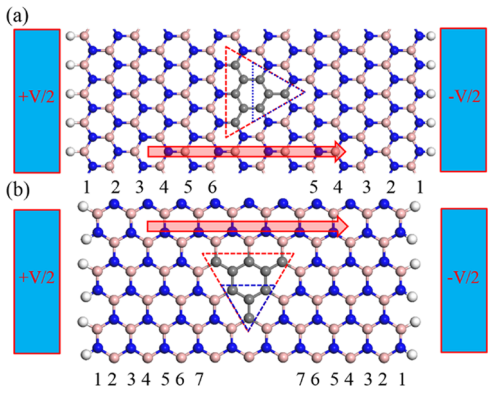

Figure 1. (a, b) Top view of the optimized geometry of zigzag and armchair CBNNRs. Optimized geometry of (a) T1-C_{3B1N} and T1-C_{6B3N} zigzag CBNNRs and (b) T2-C_{1B3N} and T2-C_{3B6N} armchair CBNNRs, respectively. The red and blue balls present boron and nitrogen atoms, respectively. The positive direction of the *E*-field is denoted by a red arrow, shown in (a) and (b) for subsequent discussions.

The corresponding optimized lattice parameter along a periodic direction of the zigzag nanoribbon is b = 12.586 Å, whereas this value is b = 13.075 Å for the armchair nanoribbon. Following a routine, we use the following notations: CB (CN) means that one B (N) atom is substituted with one C atom; C_{3B1N} means that a triangular graphene flake is formed by substituting 3 B atoms and 1 N atom with 4 C atoms, as illustrated in Figure 1. (1) T1-$C_{\alpha B\beta N}$ ($\alpha > \beta$) and (2) T2-$C_{\alpha B\beta N}$ ($\alpha < \beta$); here, two triangular graphene flakes with the same size are introduced into BNNRs through different embedding patterns, as shown in Figure 1a,b, respectively. For Figure 1a, there are 4 and 9 C atoms in the triangle graphene flake-doped BNNR, denoted as T1-C_{3B1N} (blue triangle) and T1-C_{6B3N} (red triangle), respectively. For Figure 1b, there are 4 and 9 C atoms in the triangle graphene flake-doped BNNR, denoted as T2-C_{1B3N} (blue triangle), T2-C_{3B6N} (red triangle), respectively.

3.2. Electronic Structure of Zigzag and Armchair CBNNRs. In the above section, we have optimized the geometry of the zCBNNRs and we now focus on the electronic properties. The band structure and density of states (DOS) of 6-T1-C_{3B1N}-6 and 6-T2-C_{1B3N}-6 zCBNNRs are calculated by the PBE functional, shown in Figure 2a−d, respectively. From the band structure, we can find that 6-T1-C_{3B1N}-6 zCBNNR is an indirect band gap semiconductor. The doped carbon flake tunes the BNNRs from a semiconductor of wide band gap of 4.7 eV to a semiconductor with a smaller band gap of 0.70 eV. The valence band maximum (VBM) is located at *X* point, whereas the conduction band minimum (CBM) is located at Γ point, in the irreducible Brillouin zone, indicating that the electrons could not be directly photoexcited from the VBM to the CBM. For 6-T1-C_{3B1N}-6 zCBNNR, the occupied states near the Fermi level are mainly contributed by spin-α electrons

DOI: 10.1021/acsomega.9b00752
ACS Omega 2019, 4, 10293−10301

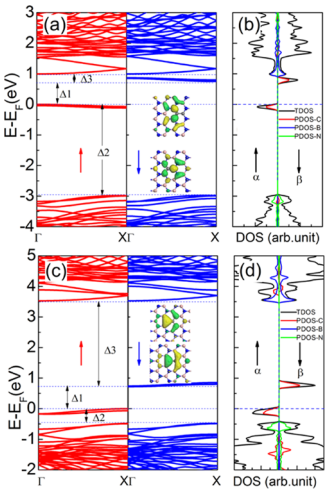

Figure 2. (a–d) Spin-polarized band structures and PDOS of zCBNNRs. Band structures of (a) 6-T1-C_{3B1N}-6 and (c) 6-T2-C_{1B3N}-6 zCBNNRs. The red and blue lines represent the α-spin and β-spin electrons, respectively. PDOS of (b) 6-T1-C_{3B1N}-6 and (d) 6-T2-C_{1B3N}-6 CBNNRs. The black, red, blue, and green lines present the total DOS of all atoms, and partial DOS of the C, B, and N atoms, respectively. Here, the spatial distributions of the VBM and CBM at the Γ point for the 6-T1-C_{3B1N}-6 system are plotted in the panel of (a) and for the 6-T2-C_{1B3N}-6 system are plotted in the panel of (c). Here, the isovalue is set as 0.06 e/Å^3.

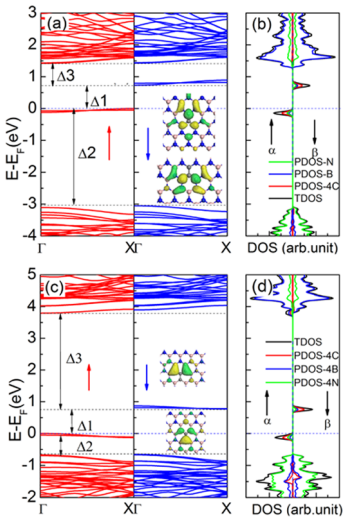

Figure 3. (a–d) Spin-polarized band structures and PDOS of aCBNNRs. Band structures of (a) 8-T1-C_{3B1N}-8 and (c) 8-T2-C_{1B3N}-8 aCBNNRs. The red and blue lines represent the α-spin and β-spin electrons, respectively. PDOS of (b) 8-T1-C_{3B1N}-8 and (d) 8-T2-C_{1B3N}-8 aCBNNRs. The black, red, blue, and green lines present the total and partial DOS of all atoms and the C, B, and N atoms, respectively. Here, the spatial distributions of the VBM (bottom) and CBM (top) at the Γ point for the 8-T1-C_{3B1N}-8 system are plotted in the panel of (a) and for the 8-T2-C_{1B3N}-8 system are plotted in the panel of (c). Here, the isovalue is 0.06 e/Å^3.

whereas the unoccupied states near the Fermi level are mainly contributed by spin-β electrons, whereas for 6-T2-C_{1B3N}-6 zCBNNR, the occupied states near the Fermi level are mainly contributed by spin-β electrons and unoccupied states near the Fermi level are mainly contributed by spin-α electrons. This means they are all typical BMS. Compared with original BNNRs, the band gap of CBNNRs is obviously decreased. To notify the reason of the reduction of the band gaps, we calculate the projected partial density of the states (PDOS) of 6-T1-C_{3B1N}-6, shown in Figure 2b. From PDOS, we can find that the states near the Fermi level are mainly contributed by four carbon atoms. This is similar with the BN nanotubes doped with carbon atoms.[52,60] For further analysis, there is an obvious hybridization (main p_z orbital hybridization) between carbon atoms and connected B or N atoms at the interface of carbon atoms.[60] The impurity states introduced by the carbon atoms lie in the original forbidden band gap.[60] So the band gap of the CBNNRs is obviously deceased. From the band structures and PDOS, the electronic properties of BNNRs are retained. From the wave function of spatial distributions of the VBM at Γ point and CBM at *X* point, the wave functions mainly localize near the carbon flakes whereas these waves functions delocalize in the nondoped perfect BNNRs.[60] And the distribution of the wave function is usually related with the chemical reaction active cites. This means that the chemical reaction active sites change to the doped carbon atoms after doping.

In the above section, the zCBNNRs are typical BMS. What about the aCBNNRs? In this section, we research the electronic properties of aCBNNRs. First, armchair BN nanoribbons (aBNNRs) doped with graphene flakes with smaller size (3 boron and 1 nitrogen atom are replaced with 4 carbon atoms) are calculated. The band structure and PDOS of 8-T1-C_{3B1N}-8 and 8-T2-C_{1B3N}-8 aCBNNRs are calculated, presented in Figure 3a–d, respectively. For 8-T1-C_{3B1N}-8, the states near the Fermi level are constituted by the different spin electrons: the VBM is contributed by spin-α electron, whereas the CBM is contributed by spin-β electron. So 8-T1-C_{3B1N}-8 is also BMS. From Figure 3a, we can get the corresponding Δ1, Δ2, and Δ3 as 0.75, 3.01, and 0.69 eV, respectively. When the triangular graphene flake is embedded in the aBNNRs, it also introduces the spin-polarized states into the original forbidden gap and this changes the wide band gap insulator to a fully spin-polarized narrow band gap semiconductor. To clarify the contribution of these states, the PDOS is also calculated, as shown in Figure 3b,d, respectively. From the PDOS, the states near the Fermi levels are mainly contributed by the carbon atoms, as shown in Figure 3b, and there is also an obvious hybridization between carbon atoms and nitrogen (T1) atoms, respectively. This hybridized state is mainly contributed by the p_z orbital. The wave functions of the VBM and CBM at Γ point also locate at the carbon flakes, which means that the chemically active sites are also transferred to the carbon atoms. This is consistent with the analysis of the PDOS. The band structure and PDOS of 8-T2-C_{1B3N}-8 aCBNNR are shown in Figure 3c,d, respectively. The band structures imply that it is also BMS, and the corresponding Δ1, Δ2, and Δ3 are 0.75, 0.65, and 3.03 eV, respectively. The states near the Fermi level are still contributed by the carbon atoms. The distributions of the wave function agree well with PDOS analysis. The VBM and CBM of 8-T1-C_{3B1N}-8 and 8-T2-C_{1B3N}-8 aCBNNRs mainly localize at the carbon atoms.

3.3. Transverse *E*-Field-Tuned Electronic Properties.

The BMS could be tuned into a spin filter by a carrier,[52] a transverse *E*-field,[61,62] and by applying a gate voltage[45,63] in previous investigations. To clearly illustrate the similar results observed in these triangular graphene flake-doped BNNRs, we take T1-C_{3B1N} and T2-C_{1B3N} as examples. The band gap of the 6-T1-C_{3B1N}-6 zCBNNR is 0.70 eV, and corresponding Δ1, Δ2,

DOI: 10.1021/acsomega.9b00752
ACS Omega 2019, 4, 10293−10301

and Δ3 are 0.70, 2.95, and 0.26 eV, respectively. Compared with Δ3, Δ1 and Δ2 are quite big, which can insure the stability of the half-metallicity under the transverse *E*-field or chemical function, whereas Δ1, Δ2, and Δ3 of 6-T1-C_{3B1N}-6 are 0.73, 0.44, and 2.77 eV, respectively. Considering that these structures are BMS with smaller band gaps means that Δ1 is quite small. And the *E*-field could tune the electronic properties of BN nanoribbons[64] and nanotubes.[54,65−68] So it is necessary to consider using the *E*-field to tune the electronic properties of zigzag and armchair CBN nanoribbons with smaller band gaps. First, the DOS of 6-T1-C_{3B1N}-6 zCBNNRs under different transverse *E*-fields is calculated and the corresponding result is shown in Figure 4. Figure 4a−d

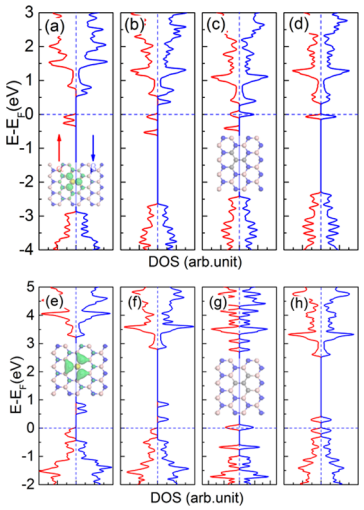

Figure 4. (a−h) DOS of 6-T1(2)-C_{mBnN}-6 zCBNNRs varies with the *E*-field, ranging from 0.02 to 0.16 eV/Å. The DOS of 6-T1-C_{3B1N}-6 with the *E*-field equal to (a) 0.02 eV/Å, (b) 0.06 eV/Å, (c) 0.12 eV/Å, and (d) 0.16 eV/Å, respectively. The DOS of 6-T2-C_{1B3N}-6 with the *E*-field of (a) 0.02 eV/Å, (b) 0.06 eV/Å, (c) 0.12 eV/Å, and (d) 0.16 eV/Å, respectively. The spin density distribution of 6-T1-C_{3B1N}-6 zCBNNR under the *E*-field of (a) 0.02 eV/Å and (b) 0.12 eV/Å is shown in the inset of (a) and (c), respectively. The spin density distribution of 6-T2-C_{1B3N}-6 under the *E*-field of (e) 0.02 eV/Å and (g) 0.12 V/Å, respectively. Here, the isovalue is 0.08 e/Å^3.

shows the DOS of the *E*-field = 0.02, 0.06, 0.12, and 0.16 V/Å, respectively. As the *E*-field increases, the corresponding band gap monotonously decreases. For the *E*-field equal to 0, the corresponding gap is 0.70 eV whereas when the *E*-field is increased to 0.02 and 0.06 V/Å, the corresponding gap decreases to 0.65 and 0.35 eV, respectively. When the *E*-field is increased to 0.12 V/Å, the corresponding gap is 0 eV. So it transforms into a metal. When the *E*-field is further increased to 0.16 V/Å, it transfers into a semiconductor with a band gap of 0.44 eV; the PDOS is shown in Figure 4d. For 6-T2-C_{1B3N}-6 zCBNNRs, the band gap is 0.76 eV without an *E*-field. When the transverse *E*-field is increased to 0.02 and 0.06 V/Å, the corresponding gap is 0.63 and 0.38 eV, shown in Figure 4e,f, respectively. As the *E*-field goes on increasing to 0.10 and 0.12 V/Å, the corresponding band gaps are 0 and 0 eV, shown in Figure 4g,h, respectively. This means that as the *E*-field increases, the band gap monotonously decreases and the system even transfers from semiconductor to metal under a stronger transverse *E*-field. Compared with perfect zigzag BNNRs, the transverse *E*-field could more effectively tune the zCBNNRs: under quite a small *E*-field, the energy gap could be more efficiently modulated.

In the following part, the electronic properties of the ribbon with increased size of the graphene flakes are also investigated. The DOS of 6-T1-C_{6B3N}-5 zCBNNR under an *E*-field of 0.02, 0.06, 0.10, 0.12, and 0.16 V/Å is calculated, and the corresponding gaps are 0.46, 0.14, 0, 0, and 0 eV, shown in Figure 5a−e, respectively. As the strength of the *E*-field goes on

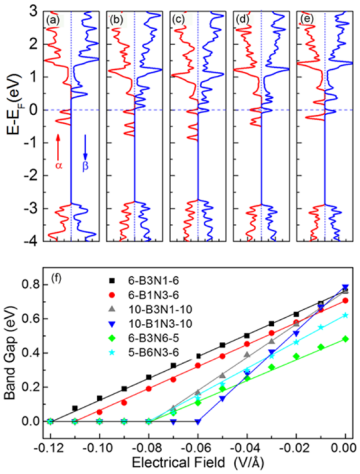

Figure 5. (a−e) DOS of 6-T1-C_{6B3N}-5 zCBNNRs with different *E*-fields is calculated by the PBE, with (a) 0.02 V/Å, (b) 0.06 V/Å, (c) 0.10 V/Å, (d) 0.12 V/Å, and (e) 0.16 V/Å, respectively. (f) The band gaps of T1-$C_{\alpha B\beta N}$ zCBNNRs change with the *E*-field. The black line with triangles, the red line with circles, the gray line with upward triangles, the blue line with downward triangles, the green line with diamonds, and the light blue line with five-pointed stars present 6-C_{3B1N}-6, 6-C_{1B3N}-6, 10-C_{3B1N}-10, 10-C_{1B3N}-10, 6-C_{3B6N}-5, and 5-C_{6B3N}-6 zCBNNRs, respectively.

increasing, the unoccupied states of the spin-β electrons are shifted down near the Fermi level. When the *E*-field is increased to 0.10 V/Å, the original unoccupied states of the spin-β electrons are shifted to the Fermi level and become partially occupied. So 6-T1-C_{6B3N}-5 zCBNNR shows half-metallicity. As the *E*-field goes on increasing to 0.12 V/Å, the fully occupied state of spin-β electrons is shifted upward and becomes partially occupied. So 6-T1-C_{6B3N}-5 becomes a common spin-polarized metal. When the *E*-field equals 0.16 V/Å, the original partial occupied states of spin-α electrons shift upward and become unoccupied, whereas the original occupied states of spin-β are still occupied. So 6-T1-C_{6B3N}-5 becomes a half-metal, conducting with the spin-β channel. In other words, the *E*-field could tune 6-T1-C_{6B3N}-5 from BMS into a half-metal used for spin filtering, conducting with either the spin-α or the spin-β channel.

The electronic properties of the CBNNRs are usually related with the position of the carbon flakes, and this condition is similar with the line defect in the graphene nanoribbon.[52] So it is quite necessary to research the effect of positon of the carbon flake on the electronic properties of CBNNRs under the transverse *E*-field. The DOSs of M-T1-C_{3B1N}-N (M + N = 12, M = 11, 9, 7, 6) 11-T1-C_{3B1N}-1, 9-T1-C_{3B1N}-3, 7-T1-C_{3B1N}-5, and 6-T1-C_{3B1N}-6 zCBNNRs under the *E*-field of 0.06 V/Å are shown in Figure 6a−d, respectively. For 11-T1-C_{3B1N}-1 without an *E*-field, the band gap is 0.16 eV. This system is transferred into half-metal under an *E*-field of 0.06 V/Å. 9-T1-C_{3B1N}-3 is a BMS with a reduced band gap of 0.60 eV, shown

DOI: 10.1021/acsomega.9b00752
ACS Omega 2019, 4, 10293−10301

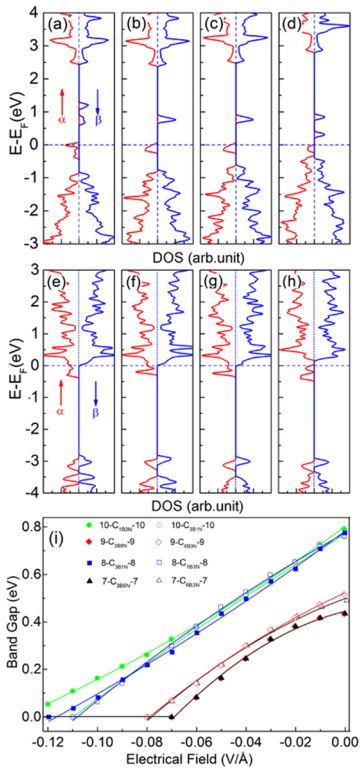

Figure 6. (a–h) DOS of M-T1-C_{3B1N}-N and M-T1-C_{6B3N}-N aCBNNRs (M + N = 12, M = 11, 9, 7, 6), respectively, under the *E*-field of −0.06 V/Å. (a–d) The DOS of M-T1-C_{3B1N}-N (M + N = 12) with M equals to (a) 11, (b) 9, (c) 7, and (d) 6, respectively. (e–h) The DOS of M-T1-C_{6B3N}-N (M + N = 18) with M equals to (e) 1, (f) 3, (g) 5, and (h) 7, respectively. (i) The evolution of the band gaps of armchair CBNNRs as a function of the external *E*-field. The green solid and hollow circles, the red solid and hollow diamonds, the blue solid and hollow rectangles, and the black solid and hollow triangles denote 10-C_{1B3N}-10, 10-C_{3B1N}-10, 9-C_{3B6N}-9, 9-C_{6B3N}-9, 8-C_{3B1N}-8, 8-C_{1B3N}-8, 7-C_{3B6N}-7, and 7-C_{6B3N}-7 aCBNNRs, respectively.

in Figure 6b. 7-T1-C_{3B1N}-5 is a BMS with a reduced band gap of 0.60 eV. 6-T1-C_{3B1N}-6 is still a BMS with a reduced band gap of 0.20 eV. When the size of the carbon flakes is further increased, the DOS of M-T1-C_{6B3N}-N (M + N = 18) under the *E*-field of 0.06 V/Å with M equal to 1, 3, 5, and 7 is shown in Figure 6e–h, respectively. From Figure 6, we can find that for M = 1, 3, and 5, the corresponding aCBNNRs are all half-metal with the spin-α channel conducting whereas the spin-β channel is insulating with band gaps of 2.80, 2.82, and 2.85 eV, respectively, whereas for M = 7, it corresponds to 7-T1-C_{6B3N}-11 zCBNNRs, which is still a semiconductor with a band gap of 0.16 eV. In other words, the position of the carbon flakes has an obvious effect on electronic properties, especially under the same strength of the *E*-field. Because the electronic properties are closely related with the VBM and CBM for the original BNNRs and different positions of the carbon flakes also affect the position of the doping states, VBM and CBM, which are determined by the carbon atoms.

aCBNNRs with different widths, patterns, and sizes of the graphene flakes under different transverse *E*-fields are also calculated, and the results are shown in Figure 6. For M-T1-C_{3B1N}-M and N-T2-C_{1B3N}-N aCBNNRs, the energy gap varies quadratically with the transverse *E*-field. M = 8, 9, and 10 are calculated. We first take M = 8 as an example, and the corresponding geometries are 8-T1-C_{3B1N}-8 and 8-T2-C_{1B3N}-8, respectively. The band gap and the transverse *E*-field follow the relationship: $y = 0.78 + 7.70x + 8.55x^2$ (T1) and $y = 0.77 + 5.75x - 12.92x^2$ (T2). For much wider CBNNRs, such as 10-T1-C_{3B1N}-10 and 10-T2-C_{1B3N}-10, the band gap and transverse *E*-field follow the relationship: $y = 0.77 + 6.25x - 6.70x^2$ and $y = 0.80 + 7.61x + 11.80x^2$. When the bigger sized carbon flakes with a triangular shape replace the boron and nitrogen atoms, i.e., 9 carbon atoms replace 6 boron and 3 nitrogen atoms, they correspond to T1-C_{6B3N} aCBNNRs. For 7-T1-C_{6B3N}-7 and 7-T2-C_{3B6N}-7, the band gap and transverse *E*-field follow the relationship: $y = 0.50 + 3.84x - 32.58x^2$ and $y = 0.44 + 2.54x - 56.43x^2$. For much wider CBNNRs, such as 9-T1-C_{6B3N}-9 and 9-T2-C_{3B6N}-9, the band gap and transverse *E*-field follow the relationship: $y = 0.52 + 4.77x - 23.26x^2$ and $y = 0.43 + 1.71x - 64.94x^2$. For the same *E*-field, such as −0.02 V/Å, the gap of 10-C_{1B3N}-10, 10-C_{3B1N}-10, 9-C_{3B6N}-9, 9-C_{6B3N}-9, 8-C_{3B1N}-8, 8-C_{1B3N}-8 7-C_{3B6N}-7, and 7-C_{6B3N}-7 CBNNRs is 0.664, 0.653, 0.383, 0.438, 0.624, 0.632, 0.379, and 0.424 eV, respectively. When the *E*-field is increased to −0.04 V/Å, the corresponding gap is 0.517, 0.515, 0.245, 0.298, 0.498, 0.527, 0.248, and 0.302 eV, respectively. For the *E*-field-0.7 V/Å, the corresponding gap is 0.328, 0.288, 0.071, 0.300, 0.272, 0.298, 0, and 0.068 eV, respectively. For the same *E*-field, the CBNNRs doped with bigger size of carbon flakes show smaller band gaps and the *E*-field shows a more obvious modulation effect.

Other CBNNRs with different size of graphene flakes are also systematically investigated, and the quadratic function relation still works for the second Stark effect. In the above section, the electronic properties under a weaker *E*-field have been investigated. What will happen when the transverse *E*-field goes on increasing? Could stronger *E*-field modulate the BMSs into SGSs or half-metal? To solve these questions, the electronic properties of 7-T1-C_{6B3N}-7 and 9-T1-C_{6B3N}-9 aCBNNRs under the stronger *E*-field are also investigated and the corresponding results are shown in Figure 7a,b,

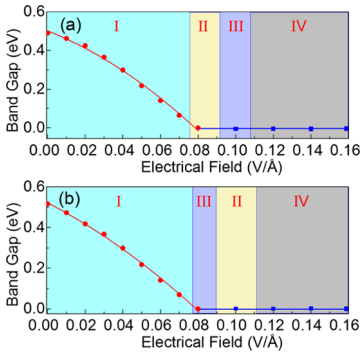

Figure 7. (a, b) Evolution of the band gap of (a) 7-T_1-C_{6B3N}-7 and (b) 9-T_2-C_{3B6N}-9 aCBNNRs as a function of the external *E*-field. The regions labeled I–IV are in the semiconductor range, metal range, SGS range, and half-metal range, respectively.

respectively. When the *E*-field is in the range (0, 0.08) V/Å, the band gap and *E*-field still follow quadratic function relation. When the *E*-field is in the range (0.08, 0.09), the CBNNRs are changed into spin-polarized metal. When the *E*-field equals to 0.10 V/Å, the system is SGS. When the *E*-field is in the range (0.11, 0.16) V/Å, the corresponding system is half-metal. In other words, 7-T1-C_{6B3N}-7 undergoes transformation from BMS, into metal, SGS, even half-metal, as the *E*-field goes on

DOI: 10.1021/acsomega.9b00752
ACS Omega 2019, 4, 10293−10301

increasing. For much wider 9-T1-C_{6B3N}-9 aCBNNRs, it changes into SGS with an *E*-field = 0.08−0.09 V/Å. When the *E*-field goes on increasing, it transfers into half-metal. So the transverse *E*-field could efficiently modulate the electronic properties of zigzag and armchair CBNNRs.

3.4. Magnetic Properties. In this part, the magnetic properties of zCBNNRs and aCBNNRs are investigated. T1-C_{3B1N} and T2-C_{1B3N} CBNNRs have 2.00 μ_B net magnetic moment (MM). The magnetic moment is mainly contributed by the carbon atoms and nearby connected B (T2) or N (T1) atoms, and more detail can be found in the Supporting Information. Taking 6-T1-C_{3B1N}-6 zigzag and 8-T2-C_{3B6N}-8 armchair CBNNRs as examples, we analyze the distribution of the magnetic moments. The carbon atoms contribute most magnetic moments to the whole system. The central carbon atom has 0.03 μ_B MM, whereas each of the three carbon atoms at the vertex of the triangle has 0.38 μ_B MM, and each nearby boron atom connected to the carbon atoms has 0.07 μ_B MM, shown in the Supporting Information. The MM is also investigated when more carbon atoms are doped into the BNNRs, such as 8-T2-C_{3B6N}-8 aCBNNR. It has 3.00 μ_B MM. Each carbon atom at the vertex of the triangle contributes 0.35 μ_B MM, and each carbon atom at the middle edge of a triangle contributes 0.26 μ_B MM, whereas other carbon atoms make little contribution, only 0.02 μ_B MM. And the common CBNNRs with bigger size of carbon flakes, such as T1-C_{6B3N} or T2-C_{3B6N}, have 3.00 μ_B MM. The carbon atoms of the same sublattice have the same spin. For T1-C_{6B3N}, six boron atom sites replaced with carbon atoms have the same spin (α) whereas three nitrogen atom sites replaced with carbon atoms show another spin (β). This means that carbon atoms belonging to the same sublattice ferromagnetically couple with the other whereas the carbon atoms belonging to the different sublattice antiferromagnetically couple with each other. This is similar to the graphene nanoribbons.[48] For T1 configuration, $\alpha - \beta$ is negative, whereas for T2, $\alpha - \beta$ is positive. For T1-T2-$C_{\alpha B\beta N}$ CBNNRs, $|\alpha - \beta|$ electrons or holes could be introduced and they have $|\alpha - \beta|$ μ_B MM, shown in Figure 8. The magnetic properties of CBNNRs could be

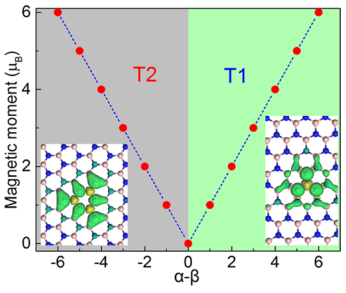

Figure 8. Magnetic moments of considered systems vary with $\alpha - \beta$. The left inset shows the spin density distribution of 8-T2-C_{3B6N}-8 aCBNNRs, and the right inset shows the spin density distribution of 6-T1-C_{3B1N}-6 zCBNNRs, respectively. Here, the isovalue is 0.08 e/Å^3.

precisely controlled by changing the size of the graphene flakes, which are doped in the BNNRs. The above predicted metal-free ferromagnetism originates from the pure 2p electrons. This ferromagnetism doesn't come from the usual 3d electrons (corresponding to the d electron magnetism), so it is named d_0 magnetism. Compared with the magnetic system of any transition metal, it has a dominant advantage for spintronics since these 2p electron systems have relatively long spin relaxation times due to the weak spin−orbit coupling.[69] Thus, the BNNRs doped with triangular graphene flakes with tunable metal-free magnetism are promising for applications in spintronic devices.

The transverse *E*-field could also tune magnetic properties of low-dimensional materials,[70] and the corresponding results are shown in the inset of Figure 4a,c,e,g, respectively. For a weaker *E*-field with 0.02 V/Å, the CBNNRs still show a spin-polarized ferromagnetic ground state and both 6-T1-C_{3B1N}-6 and 6-T2-C_{1B3N}-6 sill have a 2.00 μ_B MM, shown in the inset of Figure 4a,b, respectively. When the *E*-field gets as much as 0.12 V/Å, the transverse *E*-field fully suppresses the spin-polarization and 6-T1-C_{3B1N}-6 and 6-T2-C_{1B3N}-6 show a spin-unpolarized ground state and the total magnetic moment equals 0 μ_B, shown in the inset of Figure 4c,g, respectively.

3.5. Stability of CBN Nanoribbons. We further perform ab initio molecular dynamic (AIMD) simulations, to examine whether CBNNR is stable and whether the magnetic state could survive at room temperature (300 K). The total simulated time of one trajectory is 10 ps. As an example, we calculate the fluctuation of total energy of 6-T1-C_{3B1N}-6 and 6-T2-C_{1B3N}-6 zCBNNR, shown in Figure 9a,b, respectively. The

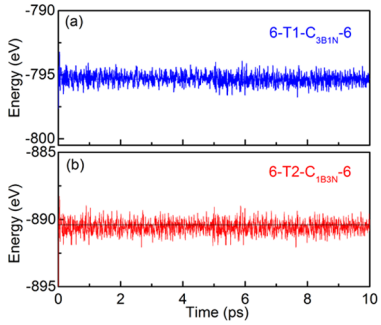

Figure 9. Total energy of (a) 6-T1-C_{3B1N}-6 and (b) of 6-T2-C_{1B3N}-6 zCBNNR as a function of MD simulation time at 300 K.

results indicate that 6-T1-C_{3B1N}-6 and 6-T2-C_{1B3N}-6 zCBNNR are stable at room temperature. During the simulation, the ribbon maintains the planar geometry without obvious distortion. This is caused by the binding energies of the C−B (393 kJ/mol), C−N (305 kJ/mol), and C−C (332 kJ/mol) bonds being much larger than the thermal energy at room temperature. Similar results were also observed in the case of CBN nanotubes.[60] The total energy oscillates around −795.366 eV during 10 ps, with the amplitude being about 0.015 eV per atom for 6-T1-C_{3B1N}-6, whereas for 6-T2-C_{1B3N}-6, the total energy oscillates around −890.323 eV, with the amplitude being about 0.016 eV per atom. We also check the snapshots of the geometries during the simulated time, and the geometries still remain planar, without obvious distortion in the stronger chemical bonding. For T1-C_{3B1N} and T2-C_{1B3N}, the total magnetic moments remain at nearly 2.00 μ_B during the simulated time, without obvious change, and the total magnetic moments remain nearly 3.00 μ_B during the simulated time for T1-C_{6B3N} and T2-C_{3B6N} zCBNNRs.

4. CONCLUSIONS

In conclusion, we examine the geometry and electronic and magnetic properties of CBNNRs with first-principles calculations. The triangular graphene flakes are embedded in BNNRs, and the corresponding CBNNRs become BMSs. The

DOI: 10.1021/acsomega.9b00752
ACS Omega 2019, 4, 10293−10301

transverse *E*-field could effectively tune the electronic properties: the gaps of zCBNNRs change linearly with the transverse *E*-field for the first-order Stark effect, whereas for aCBNNRs, the gap change varies quadratically with the electric fields for the second-order Stark effect. The transverse *E*-field could tune zCBNNRs and aCBNNRs from BMS to SGS or half-metal. The position of the graphene flakes has an effect on the electronic properties under the same *E*-field. The carbon atoms also introduce local magnetic moments, which are determined by the size of the carbon flakes. Finally, the structural and magnetic stability at room temperature are confirmed by AIMD. Our work offers a feasible strategy to design and modulate carbon, boron, and nitrogen nanostructures with different properties for nanoelectronic and spintronic applications.

■ ASSOCIATED CONTENT

Supporting Information

The Supporting Information is available free of charge on the ACS Publications website at DOI: 10.1021/acsomega.9b00752.

Materials, magnetic moment distribution of (a) 6-T1-C_{3B1N}-6 zigzag and (b) 8-T2-C_{3B6N}-8 armchair CBNNRs, band structure of 6-T1-C_{6B3N}-5 zCBNNR under certain transverse *E*-fields (PDF), the band structure of the M-T1-C_{1B3N}-N (M+N=12) CBNNRs, (a) 0-T1-C_{1B3N}-12, (b) 1-T1-C_{1B3N}-11, (c) 2-T1-C_{1B3N}-10, (d) 3-T1-C_{1B3N}-9, (e) 4-T1-C_{1B3N}-8, (f) 5-T1-C_{1B3N}-7 zigzag CBNNRs, respectively.

■ AUTHOR INFORMATION

Corresponding Author

*E-mail: zyguan@tsinghua.edu.cn. Tel: +86-010-62772784. Fax: +86-62772784.

ORCID

Zhaoyong Guan: 0000-0002-5304-028X

Shuanglin Hu: 0000-0001-9729-5500

Notes

The authors declare no competing financial interest.

■ ACKNOWLEDGMENTS

We thank Dr. Xingxing Li and Professor Wenhui Duan for useful discussion. This work was partially supported by a financial support from the President foundation of China Academy of Engineering Physics (YZJJLX2016004) and the National Key Research and Development Program of China (under Grant No. 2016YFB0201203). The computational resources from Shanghai Supercomputer Center, National Supercomputing Centers of Guangzhou, and supercomputer Centers of Tsinghua University are acknowledged.

■ REFERENCES

(1) Novoselov, K. S.; Geim, A. K.; Morozov, S. V.; Jiang, D.; Zhang, Y.; Dubonos, S. V.; Grigorieva, I. V.; Firsov, A. A. Electric Field Effect in Atomically Thin Carbon Films. *Science* **2004**, *306*, 666−669.

(2) Neto, A. H. C.; Guinea, F.; Peres, N. M. R.; Novoselov, K. S.; Geim, A. K. The Electronic Properties of Graphene. *Rev. Mod. Phys.* **2009**, *81*, 109.

(3) Bonaccorso, F.; Sun, Z.; Hasan, T.; Ferrari, A. C. Graphene Photonics and Optoelectronics. *Nat. Photonics* **2010**, *4*, 611−622.

(4) Geim, A. K. Graphene: Status and Prospects. *Science* **2009**, *324*, 1530−1534.

(5) Watanabe, K.; Taniguchi, T.; Kanda, H. Direct-Bandgap Properties and Evidence for Ultraviolet Lasing of Hexagonal Boron Nitride Single Crystal. *Nat. Mater.* **2004**, *3*, 404−409.

(6) Lin, Y.; Connell, J. W. Advances in 2d Boron Nitride Nanostructures: Nanosheets, Nanoribbons, Nanomeshes, and Hybrids with Graphene. *Nanoscale* **2012**, *4*, 6908−6939.

(7) Golberg, D.; Bando, Y.; Huang, Y.; Terao, T.; Mitome, M.; Tang, C.; Zhi, C. Boron Nitride Nanotubes and Nanosheets. *ACS Nano* **2010**, *4*, 2979−2993.

(8) Butler, S. Z.; et al. Progress, Challenges, and Opportunities in Two-Dimensional Materials Beyond Graphene. *ACS Nano* **2013**, *7*, 2898−2926.

(9) Rao, C. N. R.; Gopalakrishnan, K. Borocarbonitrides, Bxcynz: Synthesis, Characterization, and Properties with Potential Applications. *ACS Appl. Mater. Interfaces* **2017**, *9*, 19478−19494.

(10) Song, L.; Liu, Z.; Reddy, A. L. M.; Narayanan, N. T.; Taha-Tijerina, J.; Peng, J.; Gao, G.; Lou, J.; Vajtai, R.; Ajayan, P. M. Binary and Ternary Atomic Layers Built from Carbon, Boron, and Nitrogen. *Adv. Mater.* **2012**, *24*, 4878−4895.

(11) Wang, H.; Yajuan, Z.; Yong, X.; Xiaohua, M.; Xingwang, Z. Recent Progress in Synthesis of Two-Dimensional Hexagonal Boron Nitride. *J. Semicond.* **2017**, *38*, No. 031003.

(12) Ye, J.; Rothhaar, U.; Oechsner, H. Conditions for the Formation of Cubic Boron Nitride Films by Rf Magnetron Sputtering. *Surf. Coat. Technol.* **1998**, *105*, 159−164.

(13) Glavin, N. R.; Jespersen, M. L.; Check, M. H.; Hu, J.; Hilton, A. M.; Fisher, T. S.; Voevodin, A. A. Synthesis of Few-Layer, Large Area Hexagonal-Boron Nitride by Pulsed Laser Deposition. *Thin Solid Films* **2014**, *572*, 245−250.

(14) Yi, Q.; Zhao, T.; Wang, B.; Yang, J.-F. Influence of Deposition and in Situ Annealing Time on Composition and Optical Band Gap of H-BN Films Deposited by Pecvd. *J. Inorg. Mater.* **2014**, *29*, 729−734.

(15) Park, K. S.; Lee, D. Y.; Kim, K. J.; Moon, D. W. Observation of a Hexagonal BNSurface Layer on the Cubic BN Film Grown by Dual Ion Beam Sputter Deposition. *Appl. Phys. Lett.* **1997**, *70*, 315−317.

(16) Zhang, W. J.; Jiang, X.; Matsumoto, S. High-Quality, Faceted Cubic Boron Nitride Films Grown by Chemical Vapor Deposition. *Appl. Phys. Lett.* **2001**, *79*, 4530−4532.

(17) Chan, C. Y.; Zhang, W. J.; Matsumoto, S.; Bello, I.; Lee, S. T. A Nanoindentation Study of Thick CBN Films Prepared by Chemical Vapor Deposition. *J. Cryst. Growth* **2003**, *247*, 438−444.

(18) Zhang, W. J.; Bello, I.; Lifshitz, Y.; Chan, K. M.; Wu, Y.; Chan, C. Y.; Meng, X. M.; Lee, S. T. Thick and Adherent Cubic Boron Nitride Films Grown on Diamond Interlayers by Fluorine-Assisted Chemical Vapor Deposition. *Appl. Phys. Lett.* **2004**, *85*, 1344−1346.

(19) Shi, Y.; et al. Synthesis of Few-Layer Hexagonal Boron Nitride Thin Film by Chemical Vapor Deposition. *Nano Lett.* **2010**, *10*, 4134−4139.

(20) Sutter, P.; Lahiri, J.; Albrecht, P.; Sutter, E. Chemical Vapor Deposition and Etching of High-Quality Monolayer Hexagonal Boron Nitride Films. *ACS Nano* **2011**, *5*, 7303−7309.

(21) Kim, K. K.; et al. Synthesis of Monolayer Hexagonal Boron Nitride on Cu Foil Using Chemical Vapor Deposition. *Nano Lett.* **2012**, *12*, 161−166.

(22) Lee, K. H.; Shin, H.-J.; Lee, J.; Lee, I.-y.; Kim, G.-H.; Choi, J.-Y.; Kim, S.-W. Large-Scale Synthesis of High-Quality Hexagonal Boron Nitride Nanosheets for Large-Area Graphene Electronics. *Nano Lett.* **2012**, *12*, 714−718.

(23) Redlich, P.; Loeffler, J.; Ajayan, P.; Bill, J.; Aldinger, F.; Rühle, M. BCNNanotubes and Boron Doping of Carbon Nanotubes. *Chem. Phys. Lett.* **1996**, *260*, 465−470.

(24) Carroll, D.; Redlich, P.; Blase, X.; Charlier, J.-C.; Curran, S.; Ajayan, P.; Roth, S.; Rühle, M. J. P. R. L. Effects of Nanodomain Formation on the Electronic Structure of Doped Carbon Nanotubes. *Phys. Rev. Lett.* **1998**, *81*, No. 2332.

(25) Ulrich, S.; Ehrhardt, H.; Theel, T.; Schwan, J.; Westermeyr, S.; Scheib, M.; Becker, P.; Oechsner, H.; Dollinger, G.; Bergmaier, A. Phase Separation in Magnetron Sputtered Superhard BCN Thin Films. *Diamond Relat. Mater.* **1998**, *7*, 839−844.

DOI: 10.1021/acsomega.9b00752
ACS Omega 2019, 4, 10293−10301

(26) Choi, J.; Kim, Y.-H.; Chang, K.-J.; Tománek, D. J. P. R. B. Itinerant Ferromagnetism in Heterostructured C/BN Nanotubes. *Phys. Rev. B* **2003**, *67*, No. 125421.
(27) Ma, R.; Golberg, D.; Bando, Y.; Sasaki, T. Syntheses and Properties of B−C−N and BN Nanostructures. *Philos. Trans. R. Soc., A* **2004**, *362*, 2161−2186.
(28) Enouz, S.; Stéphan, O.; Cochon, J.-L.; Colliex, C.; Loiseau, A. C−BN Patterned Single-Walled Nanotubes Synthesized by Laser Vaporization. *Nano Lett.* **2007**, *7*, 1856−1862.
(29) Yuge, K.; Seko, A.; Koyama, Y.; Oba, F.; Tanaka, I. First-Principles-Based Phase Diagram of the Cubic Bnc Ternary System. *Phys. Rev. B* **2008**, *77*, No. 094121.
(30) Huang, B.; Si, C.; Lee, H.; Zhao, L.; Wu, J.; Gu, B.-L.; Duan, W. Intrinsic Half-Metallic BN−C Nanotubes. *Appl. Phys. Lett.* **2010**, *97*, No. 043115.
(31) Huang, Z.; Crespi, V. H.; Chelikowsky, J. R. J. P. R. B. Electronic Properties of Mixed-Phase Graphene/H-BN Sheets Using Real-Space Pseudopotentials. *Appl. Phys. Lett.* **2013**, *88*, No. 235425.
(32) Guilhon, I.; Marques, M.; Teles, L. K.; Bechstedt, F. Optical Absorbance and Band-Gap Engineering of $(BN)_{(1-X)}(C\text{-}2)_{(X)}$ Two-Dimensional Alloys: Phase Separation and Composition Fluctuation Effects. *Phys. Rev. B* **2017**, *95*, No. 035407.
(33) da Rocha Martins, J.; Chacham, H. Disorder and Segregation in B−C−N Graphene-Type Layers and Nanotubes: Tuning the Band Gap. *ACS Nano* **2011**, *5*, 385−393.
(34) Kim, G.; et al. Planar and Van Der Waals Heterostructures for Vertical Tunnelling Single Electron Transistors. *Nat. Commun.* **2019**, *10*, No. 230.
(35) Ci, L.; et al. Atomic Layers of Hybridized Boron Nitride and Graphene Domains. *Nat. Mater.* **2010**, *9*, 430.
(36) Berseneva, N.; Krasheninnikov, A. V.; Nieminen, R. M. Mechanisms of Postsynthesis Doping of Boron Nitride Nanostructures with Carbon from First-Principles Simulations. *Phys. Rev. Lett.* **2011**, *107*, No. 035501.
(37) Han, W.-Q.; Yu, H.-G.; Liu, Z. Convert Graphene Sheets to Boron Nitride and Boron Nitride−Carbon Sheets Via a Carbon-Substitution Reaction. *Appl. Phys. Lett.* **2011**, *98*, No. 203112.
(38) Lu, J.; Zhang, K.; Feng Liu, X.; Zhang, H.; Chien Sum, T.; Castro Neto, A. H.; Loh, K. P. Order−Disorder Transition in a Two-Dimensional Boron−Carbon−Nitride Alloy. *Nat. Commun.* **2013**, *4*, No. 2681.
(39) Liu, L.; Park, J.; Siegel, D. A.; McCarty, K. F.; Clark, K. W.; Deng, W.; Basile, L.; Idrobo, J. C.; Li, A.-P.; Gu, G. Heteroepitaxial Growth of Two-Dimensional Hexagonal Boron Nitride Templated by Graphene Edges. *Science* **2014**, *343*, 163−167.
(40) Wei, X.; Wang, M.-S.; Bando, Y.; Golberg, D. Electron-Beam-Induced Substitutional Carbon Doping of Boron Nitride Nanosheets, Nanoribbons, and Nanotubes. *ACS Nano* **2011**, *5*, 2916−2922.
(41) Ilyasov, V. V.; Meshi, B. C.; Nguyen, V. C.; Ershov, I. V.; Nguyen, D. C. Tuning the Band Structure, Magnetic and Transport Properties of the Zigzag Graphene Nanoribbons/Hexagonal Boron Nitride Heterostructures by Transverse Electric Field. *J. Chem. Phys.* **2014**, *141*, No. 014708.
(42) Pham, K. D.; Hieu, N. N.; Phuc, H. V.; Fedorov, I. A.; Duque, C. A.; Amin, B.; Nguyen, C. V. Layered Graphene/Gas Van Der Waals Heterostructure: Controlling the Electronic Properties and Schottky Barrier by Vertical Strain. *Appl. Phys. Lett.* **2018**, *113*, No. 171605.
(43) Phuc, H. V.; Hieu, N. N.; Hoi, B. D.; Nguyen, C. V. Interlayer Coupling and Electric Field Tunable Electronic Properties and Schottky Barrier in a Graphene/Bilayer-Gase Van Der Waals Heterostructure. *Phys. Chem. Chem. Phys.* **2018**, *20*, 17899−17908.
(44) Perdew, J. P.; Burke, K.; Ernzerhof, M. Generalized Gradient Approximation Made Simple. *Phys. Rev. Lett.* **1996**, *77*, 3865−3868.
(45) Li, X.; Wu, X.; Li, Z.; Yang, J.; Hou, J. G. Bipolar Magnetic Semiconductors: A New Class of Spintronics Materials. *Nanoscale* **2012**, *4*, 5680−5685.
(46) Wang, X. L. Proposal for a New Class of Materials: Spin Gapless Semiconductors. *Phys. Rev. Lett.* **2008**, *100*, No. 156404.
(47) Wang, X.; Peleckis, G.; Zhang, C.; Kimura, H.; Dou, S. Colossal Electroresistance and Giant Magnetoresistance in Doped PbPdO2 Thin Films. *Adv. Mater.* **2009**, *21*, 2196−2199.
(48) Wang, X.; Li, T.; Cheng, Z.; Wang, X.-L.; Chen, H. Recent Advances in Dirac Spin-Gapless Semiconductors. *Appl. Phys. Rev.* **2018**, *5*, No. 041103.
(49) Pickett, W. E.; Moodera, J. S. Half Metallic Magnets. *Phys. Today* **2001**, *54*, 39−44.
(50) Son, Y. W.; Cohen, M. L.; Louie, S. G. Half-Metallic Graphene Nanoribbons. *Nature* **2006**, *444*, 347−349.
(51) Ataca, C.; Sahin, H.; Ciraci, S. Stable, Single-Layer MX_2 Transition-Metal Oxides and Dichalcogenides in a Honeycomb-Like Structure. *J. Phys. Chem. C* **2012**, *116*, 8983−8999.
(52) Guan, Z.; Si, C.; Hu, S.; Duan, W. First-Principles Study of Line-Defect-Embedded Zigzag Graphene Nanoribbons: Electronic and Magnetic Properties. *Phys. Chem. Chem. Phys.* **2016**, *18*, 12350−12356.
(53) Park, C.-H.; Louie, S. G. Energy Gaps and Stark Effect in Boron Nitride Nanoribbons. *Nano Lett.* **2008**, *8*, 2200−2203.
(54) Khoo, K. H.; Mazzoni, M. S. C.; Louie, S. G. Tuning the Electronic Properties of Boron Nitride Nanotubes with Transverse Electric Fields: A Giant Dc Stark Effect. *Phys. Rev. B* **2004**, *69*, No. 201401.
(55) Zhuhua, Z.; Wanlin, G. Energy-Gap Modulation of BN Ribbons by Transverse Electric Fields: First-Principles Calculations. *Phys. Rev. B* **2008**, *77*, No. 075403.
(56) Delley, B. An All-Electron Numerical Method for Solving the Local Density Functional for Polyatomic Molecules. *J. Chem. Phys.* **1990**, *92*, 508−517.
(57) Delley, B. From Molecules to Solids with the $Dmol^3$ Approach. *J. Chem. Phys.* **2000**, *113*, 7756−7764.
(58) Monkhorst, H. J.; Pack, J. D. Special Points for Brillouin-Zone Integrations. *Phys. Rev. B* **1976**, *13*, 5188−5192.
(59) Topsakal, M.; Aktürk, E.; Ciraci, S. First-Principles Study of Two- and One-Dimensional Honeycomb Structures of Boron Nitride. *Phys. Rev. B* **2009**, *79*, No. 115442.
(60) Guan, Z. Y.; Wang, W. Y.; Huang, J.; Wu, X. J.; Li, Q. X.; Yang, J. L. Tunable Electronic and Magnetic Properties of Graphene Flake-Doped Boron Nitride Nanotubes. *J. Phys. Chem. C* **2014**, *118*, 28616−28624.
(61) Kang, J.; Fengmin, W.; Jingbo, L. Modulating the Bandgaps of Graphdiyne Nanoribbons by Transverse Electric Fields. *J. Phys.: Condens. Matter* **2012**, *24*, No. 165301.
(62) Kumar, S. B.; Guo, J. Transversal Electric Field Effect in Multilayer Graphene Nanoribbon. *Appl. Phys. Lett.* **2011**, *98*, No. 222101.
(63) Menezes, M. G.; Capaz, R. B. Half-Metallicity Induced by Charge Injection in Hexagonal Boron Nitride Clusters Embedded in Graphene. *Phys. Rev. B* **2012**, *86*, No. 195413.
(64) Tang, Q.; Zhen, Z.; Panwen, S.; Zhongfang, C. Band Gap Engineering of BN Sheets by Interlayer Dihydrogen Bonding and Electric Field Control. *ChemPhysChem* **2013**, *14*, 1787−92.
(65) Akdim, B.; Pachter, R. Bandgap Tuning of a (6,6) Boron Nitride Nanotube by Analyte Physisorption and Application of a Transverse Electric Field: A DFT Study. *IEEE Trans. Nanotechnol.* **2011**, *10*, 1089−1092.
(66) Chegel, R.; Behzad, S. Electro-Optical Properties of Zigzag and Armchair Boron Nitride Nanotubes under a Transverse Electric Field: Tight Binding Calculations. *J. Phys. Chem. Solids* **2012**, *73*, 154−161.
(67) Chegel, R.; Behzad, S.; Ahmadi, E. Effects of Electric and Magnetic Fields on the Electronic Properties of Zigzag Carbon and Boron Nitride Nanotubes. *Solid State Sci.* **2012**, *14*, 456−464.
(68) Freitas, A.; Azevedo, S.; Kaschny, J. R. Effects of a Transverse Electric Field on the Electronic Properties of Single- and Multi-Wall BN Nanotubes. *Solid State Commun.* **2013**, *153*, 40−45.
(69) Sanvito, S. Molecular Spintronics. *Chem. Soc. Rev.* **2011**, *40*, 3336−3355.
(70) Son, Y.-W.; Cohen, M. L.; Louie, S. G. Half-Metallic Graphene Nanoribbons. *Nature* **2006**, *444*, 347.

DOI: 10.1021/acsomega.9b00752
ACS Omega 2019, 4, 10293−10301